JOURNAL OF CATALYSIS 138, 570–587 (1992)

Non-Faradaic Electrochemical Modification of Catalytic Activity

5. Oxygen Chemisorption on Silver

S. BEBELIS AND C. G. VAYENAS[1]

Institute of Chemical Engineering and High Temperature Chemical Processes, Department of Chemical Engineering, University of Patras, Patras GR 26110 Greece

Received November 13, 1991; revised May 26, 1992

The technique of isothermal surface titration was used to investigate the chemisorptive properties of porous Ag films deposited on Y_2O_3-doped ZrO_2 in a solid electrolyte cell. It was found that the chemisorptive properties of Ag can be influenced in a pronounced and reversible manner upon polarizing electrochemically the metal–solid electrolyte interface. Decreasing catalyst work function has very little effect on subsurface oxygen but strengthens significantly the Ag–atomic oxygen chemisorptive bond, as inferred both by the observed pronounced increases in the rate of oxygen adsorption and in the equilibrium oxygen coverage and by the observed significant decrease in the rate of atomic oxygen desorption. The results are consistent with the previously proposed interpretation of the NEMCA effect and show that solid electrolytes can be used as active catalyst supports to alter significantly the chemisorptive and catalytic properties of metals.

INTRODUCTION

The effect of non-Faradaic electrochemical modification of catalytic activity (NEMCA) has been described in a number of recent papers (*1–17*). In brief, it has been found that the catalytic activity and selectivity of porous metal films interfaced with solid electrolytes can be altered in a dramatic, reversible, and, to some extent, predictable manner (*1, 2*). This is accomplished by applying currents or voltages to solid electrolyte cells of the type

gaseous reactants, metal catalyst | solid electrolyte | counter electrode, air or auxiliary gas mixture (1)

and, consequently, by supplying or removing ions (e.g., O^{2-}, Na^+) to or from the polarizable catalyst–solid electrolyte interface (*1–17*). The steady-state increase in the catalytic reaction rate can be a factor of 70 higher than the regular, i.e., open-circuit catalytic rate and a factor of 3×10^5 higher than the rate of supply or removal of ions (*1–17*). The term "electrochemical promotion in catalysis" has also been proposed to describe NEMCA (*18*), which has been studied already for some 20 catalytic reactions on Pt, Pd, Rh, Ag, and Ni catalysts (*1–17*). The effect does not appear to be limited to any particular metal or solid electrolyte (*1–17*).

The main common findings of previous NEMCA studies can be summarized as follows.

I. Over wide ranges of catalyst work function $e\Phi$, typically 0.3 to 1 eV, catalytic rates depend exponentially on $e\Phi$:

$$\ln(r/r_o) = \alpha e(\Phi - \Phi^*)/k_b T, \qquad (2)$$

where r_o is the regular, i.e., open-circuit catalytic rate, α and Φ^* are reaction- and catalyst-specific constants, and k_b is Boltzmann's constant. Over the same work function ranges, catalytic activation energies

[1] Present address: Department of Chemical Engineering, Yale University, New Haven, CT 06520.

0021-9517/92 $5.00

vary linearly with $e\Phi$. The average gas-exposed catalyst surface work function $e\Phi$ can be varied conveniently by simply varying, via a potentiostat, the ohmic-drop-free catalyst potential V_{WR} with respect to a reference (R) electrode. The change $e\Delta V_{WR}$ equals $-\Delta\bar{\mu}_e$, where $\bar{\mu}_e$ is the electrochemical potential of electrons in the metal catalyst, which equals the catalyst Fermi level (*2*). Both theory (*2*, *5*, *6*) and experiments utilizing a Kelvin probe (*1*, *10*, *11*) have shown furthermore that in solid electrolyte cells with metal electrodes

$$e\Delta V_{WR} = \Delta e\Phi, \tag{3}$$

so that the catalyst work function can be varied at will and independently from the gas phase. A detailed analysis on the subject is given in a recent monograph (*2*), while a brief summary is given in the Appendix.

II. The absolute value $|\Lambda|$ of the enhancement factor Λ defined from

$$\Lambda = \Delta r/(I/2F), \tag{4}$$

where Δr is the NEMCA-induced change in catalytic rate, I is the applied current (defined positive when anions are supplied to the catalyst), and F is Faraday's constant, can be approximated by

$$|\Lambda| = 2Fr_o/I_0, \tag{5}$$

where I_0 is the exchange current of the catalyst–solid electrolyte interface (*1–17*). Thus, to study NEMCA, one must use polarizable, i.e., low I_0, metal–solid electrolyte interfaces.

III. The reaction rate relaxation time constant τ during galvanostatic transients, defined as the time required for the rate change to reach 63% of its final steady-state value when a constant current is applied between the catalyst and the counter electrode, can be approximated by

$$\tau \approx 2FN/I, \tag{6}$$

where N, expressed in metal g-atom, is the gas-exposed catalyst surface area.

The above observations have been interpreted by attributing NEMCA to the changes induced in the strengths of chemisorptive bonds of reactants and intermediates upon changing the catalyst work function via an electrochemically induced spillover of ions from (or to) the solid electrolyte to (or from) the catalyst surface (*1–17*).

The purpose of the present work is to provide a crucial test to the proposed interpretation of NEMCA by examining whether the strength of chemisorptive bonds of covalently bonded species is indeed varied under NEMCA conditions, i.e., upon polarization of the metal–solid electrolyte interface. To this end the kinetics of oxygen and ethylene adsorption on and desorption from Ag were investigated both under open-circuit conditions and during polarization of the Ag–solid electrolyte interface.

The chemisorption of oxygen and of ethylene on Ag was chosen for this test study because of the industrial importance of the epoxidation of ethylene and also because this chemisorption system, despite its complexity, has been studied extensively both on clean and on promoted Ag surfaces (*19–37*). It is also worth noting that the Ag-catalyzed ethylene epoxidation has already been shown to exhibit the NEMCA effect both with O^{2-}-conducting (*2*, *13*, *38*) and with Na^+-conducting solid electrolytes (*2*, *39*).

Several forms of oxygen have been found to exist on Ag surfaces. These include (I) molecularly adsorbed oxygen, which is rather inactive and has been shown by Lambert and co-workers to behave as a "spectator" species (*19*, *33*, *34*), (II) atomic oxygen, which is currently believed to be the reactive oxygen species for both ethylene epoxidation and complete oxidation (*19*, *22*, *40*), and (III) subsurface oxygen, which appears to be necessary for obtaining high selectivity to epoxide, although it does not directly participate in catalytic events (*19*, *37*). Ethylene adsorption on Ag is weak (*19–21*) but is enhanced in the presence of preadsorbed oxygen (*41*).

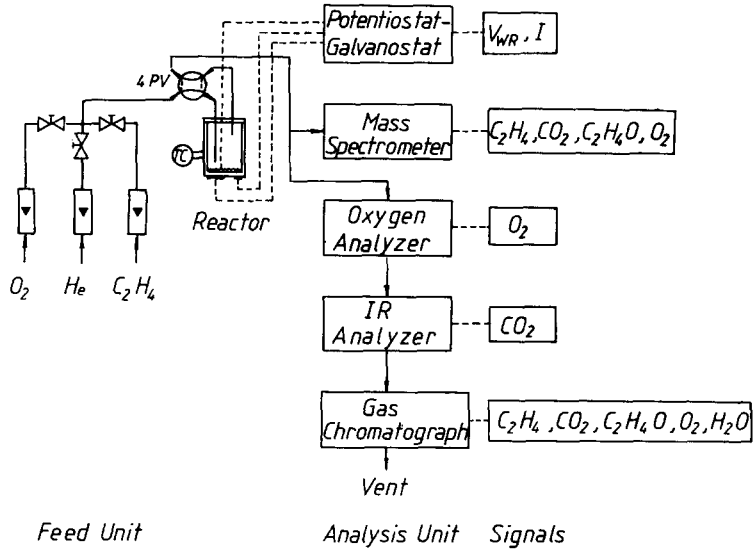

FIG. 1. Schematic diagram of the apparatus.

EXPERIMENTAL

The experimental apparatus shown schematically in Fig. 1 and utilizing on-line mass spectrometry, IR spectroscopy, gas chromatography, and an electrochemical oxygen analyzer (Teledyne 326 RA) for reactor inlet and effluent analysis is of the same type used in previous NEMCA studies and has been described in detail elsewhere (*2–7*). The 8 mol% Y_2O_3-stabilized ZrO_2 (YSZ) reactor shown in Fig. 2 and described in detail elsewhere has a volume of 30 cm^3 and has been shown to be well-mixed (CSTR) over the range of flow rates used in the present study, i.e., 3 to 7 cm^3 STP/s. Special precautions were taken to minimize dead volumes by using zero-dead-volume Nupro on–off valves and short connecting stainless-steel lines between the valves and the reactor. Reactants were Messer Griesheim certified standards of C_2H_4 in He, O_2 in He, and ultrapure (99.999%) He.

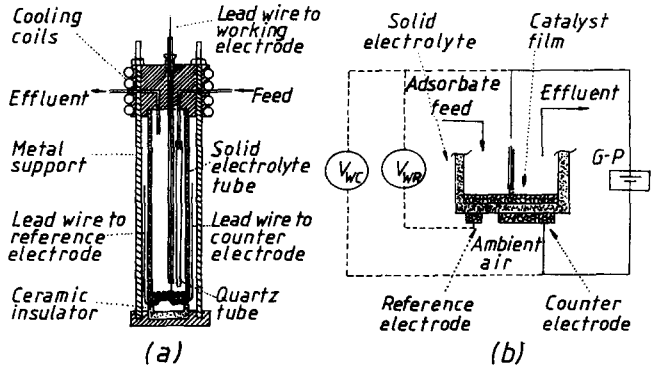

FIG. 2. Solid electrolyte catalytic reactor (a) and catalyst and auxiliary electrodes configuration (b). G–P, galvanostat–potentiostat.

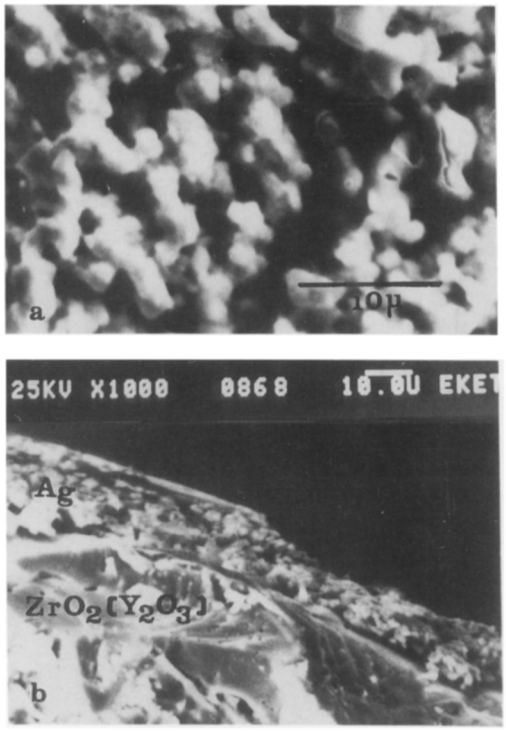

FIG. 3. Scanning electron micrographs of the top side of the porous Ag catalyst film (a) and of a section perpendicular to the Ag catalyst–yttria stabilized zirconia (YSZ) interface (b).

Catalyst film. The porous Ag catalyst film deposited on the inside bottom wall of the YSZ tube had a thickness of ~10 μm, a superficial surface area of 2 cm^2, and a true surface area of 0.13 m^2 as estimated by the surface titration technique described below. Figure 3a shows a scanning electron micrograph (SEM) of the top view of a Ag catalyst film. A cross section of the Ag–YSZ interface is depicted in Fig. 3b.

The Ag catalyst film was prepared by depositing a thin coating of a Ag solution in butyl acetate (GC electronics) followed by drying at 80°C and calcining at 650°C as described in previous papers where catalyst preparation and characterization details are presented (*2, 6, 13, 49*). The same procedure was used to deposit two similar Ag films on the air-exposed side of the flat bottom of the YSZ tube (Fig. 2). The larger of these two films was used as a counter electrode and the smaller one as a reference electrode. Both the counter and the reference Ag electrodes were exposed to ambient air.

Galvanostatic operation of the cell. When a galvanostat (in this work an AMEL 553 galvanostat–potentiostat) is used to apply a constant current between the counter electrode and the catalyst, oxygen anions O^{2-} are supplied to ($I > 0$) or removed from ($I < 0$) the catalyst–solid electrolyte interface at a rate $I/2F$. At this interface the electrocatalytic reaction

$$O^{2-} \leftrightharpoons O(a) + 2e^-, \qquad (7)$$

takes place, where O(a) stands for oxygen adsorbed on Ag. When oxygen is practically insoluble in the metal, then the above reaction takes place mainly at the three-phase boundaries, metal–YSZ–gas (*2, 42–44*). However, when oxygen has a finite solubility in the metal electrode, as in the present case of Ag (*45*), the deelectronation of O^{2-} can also take place significantly at the two-phase boundaries, Ag–YSZ, followed by diffusion of dissolved oxygen through the Ag electrode to the gas-exposed, i.e., catalytically active, electrode surface, again resulting on the surface as chemisorbed oxygen O(a). In either case the exchange current I_0 is defined as the rate of the forward (or backward) reaction (*7*) under open-circuit conditions, i.e., when no net current crosses the interface (*2, 5, 6*). The parameter I_0 can be determined easily from current-overpotential measurements as described in detail elsewhere (*2, 5, 6*) and provides a measure of the nonpolarizability of catalyst–YSZ interface. Contrary to fuel cell applications where high I_0 values are desirable to minimize polarization losses (*2, 15*), for NEMCA applications low I_0, i.e., highly polarizable, metal–solid electrolyte interfaces must be used (*1–17*).

The exchange current I_0, together with the anodic and cathodic transfer coefficients α_a and α_c, can be extracted from standard Tafel plots as described in detail elsewhere

(*2*, *5*, *6*). In the present work the I_0 value of the Ag–YSZ interface was 140 μA at 435°C where most of the surface titration experiments were performed. The α_a and α_c values were 0.24 and 0.07, respectively. These I_0, α_a, and α_c values were measured with the catalyst exposed to P_{O_2} = 3.15 kPa and $P_{C_2H_4}$ = 2.4 kPa. Although I_0, α_a, and α_c are dependent on gaseous composition (*2*, *44*) one can use the above average values to estimate the catalyst overpotential $\eta = \Delta V_{WR}$ for any value of I via the Butler–Volmer equation (*2*, *5*, *6*),

$$I/I_0 = \exp(\alpha_a F\eta/RT) - \exp(-\alpha_c F\eta/RT). \quad (8)$$

Equation (8) implies that when $I > 0$, $\eta = \Delta V_{WR} > 0$; i.e., the catalyst potential V_{WR} (with respect to the reference electrode) increases above its open-circuit value V^{o}_{WR}. As shown recently both theoretically (*2*, *5*, *6*) and experimentally by means of a Kelvin probe (*1*, *11*),

$$e\Delta V_{WR} = \Delta e\Phi, \quad (3)$$

where $e\Phi$ is the average catalyst surface work function. In view of Eqs. (3) and (8) it follows that when $I > 0$, $\Delta e\Phi > 0$; i.e., the catalyst surface work function increases and this increase can be computed via Eqs. (3) and (8). Physically this is because when the metal–solid electrolyte interface is polarized, i.e., when reaction (7) is slow, spillover oxide ions (most likely O^- (*2*, *4*, *5*)) are also produced at the three-phase boundaries and spill over the catalyst surface together with their compensating charge in the metal, thus forming spillover dipoles (*1–17*). The coverage of these spillover ions is low. It has been estimated (*1*, *2*) that a spillover oxide ion coverage of less than 0.05 suffices to produce a work function increase of 1 eV.

Conversely, when $I < 0$, the catalyst work function decreases. This decrease from the open-circuit value can be computed again via Eqs. (3) and (8). It physically results from a decrease in the steady-state coverage of spillover ions on the catalyst surface. Thus, by controlling I and V_{WR} one can control the catalyst work function $e\Phi$ independently from the gas phase.

Isothermal surface titration (IST) technique. The IST technique has been used in the past for measuring the surface area of metal catalyst films (*2*, *3*, *10*). Throughout the measurements the catalyst film is maintained at a fixed temperature T and the reactor effluent composition is continuously monitored via the electrochemical oxygen analyzer and a differentially pumped continuous sampling capillary system leading into the high vacuum chamber of the mass spectrometer. The procedure consists of the following three steps.

I. First the catalyst is exposed to a stream of O_2 (or C_2H_4) for a time period denoted by t_{O_2} (or t_E). In the present study certified standards of 21 mol% O_2 in He and 11 mol% C_2H_4 in He were used.

II. Then the reactor is purged with a stream of ultrapure He for a time period t_{He} at least eight times longer than the residence time of the reactor cell, which is typically 2–5 s. During t_{He}, desorption of O_2 (or C_2H_4) is taking place.

III. Subsequently the catalyst is exposed to a stream of C_2H_4 (or O_2) while the effluent composition is monitored by a mass spectrometer. The product CO_2 and ethylene oxide peaks provide a direct measure of the amount of chemisorbed oxygen (or C_2H_4) which was adsorbed on the surface after t_{He}. This amount clearly depends on t_{O_2} (or t_E) unless t_{O_2} (or t_E) is long enough for saturation, i.e., adsorption equilibrium, to be established between the gas and the catalyst surface during step I.

The IST technique has been used already (*2*, *3*, *10*) to measure catalyst surface areas. To this end t_{O_2} (or t_E) is made sufficiently long to establish surface saturation and then t_{He} is varied in a series of experiments to determine the amount of O_2 (or C_2H_4) denoted by $N_O(t_{He})$ and $N_E(t_{He})$, respectively, remaining on the surface after desorption has taken place for $t = t_{He}$. By plotting $N_O(t_{He})$ or $N_E(t_{He})$ vs t_{He} and extrapolating

to $t_{He} = 0$, one determines the reactive oxygen (or ethylene) catalyst uptake at saturation, denoted by $N_{O,max}$ and $N_{E,max}$, respectively. If the adsorption stoichiometry is known, one can then determine the amount of metal g-atoms on the surface or, equivalently, the catalyst surface area.

IST under catalyst polarization (NEMCA) conditions. In order to study the effect of O^{2-} electrochemical pumping, and of the concomitant Fermi level and work function changes, on the adsorption and desorption of oxygen and C_2H_4 on Ag, three different sets of experiments were performed, each involving variation of t_{O_2} (or t_E) and t_{He}:

a. Isothermal titrations under open-circuit conditions ($I = 0$)

b. Isothermal titrations under low V_{WR} and $e\Phi$ conditions ($I = -110\ \mu A$)

c. Isothermal titrations under high V_{WR} and $e\Phi$ conditions ($I = 400\ \mu A$).

In cases b and c the constant current was applied throughout steps I, II, and III. During each titration the catalyst potential V_{WR} was continuously recorded together with the effluent concentrations of O_2, C_2H_4, C_2H_4O, and CO_2. Most experiments were performed at 435°C where the selectivity to ethylene oxide was $S = 0.27$. Since S was found to be rather insensitive to reactor residence time and gaseous composition at fixed T (*38*, *39*, *48*, *50*), the AMU 44 signal was used with the known cracking patterns of C_2H_4O and CO_2 and the above selectivity value to determine the amount of reacting oxygen or ethylene.

It must be emphasized that in cases b and c oxide ions O^{2-} are removed from and supplied to the catalyst, respectively, at a rate $I/2F$. Thus in case b there is a removal of 3.4×10^{-7} g-atom O every 10 min, while in case c there is a supply of 1.2×10^{-6} g-atom O every 10 min. In case c this amount of oxygen is comparable with the reactive oxygen catalyst uptake, thus complicating data interpretation and allowing only for qualitative conclusions to be drawn. Ideally it would be desirable to carry out the experiments with a vanishingly small I_0 catalyst–YSZ interface, thus allowing catalyst polarization with extremely small I values and rendering the amount of electrochemically supplied or removed oxygen negligible in comparison with the reactive oxygen catalyst uptake. This cannot be performed practically for two reasons. First, the Ag–YSZ interfaces generally possess relatively high I_0 values even with the high catalyst sintering temperatures employed in this study (*2*, *48*). Second, if an exceedingly small I_0 value could be achieved (e.g., 0.1 μA) so that a current of 1 μA could sufficiently polarize the Ag–YSZ interface, then the ion spillover time (*1–17*) $\tau \approx 2FN_{O,max}/I$ would be of the order of hours for $N_{O,max} \sim 1.5 \times 10^{-6}$ g-atom O as in the present study; therefore, no polarization would occur during the time scale of the adsorption–desorption experiments (typically on the order of a few minutes). Consequently the $I_0 = 140\ \mu A$ value of the Ag–YSZ interface used in this study provided a reasonable compromise between these two opposing factors. It is worth pointing out that the same type of problems would be encountered if TPD rather than IST had been used in the present study. Fortunately, as shown under Results, negative current application (case b, i.e., O^{2-} removal from the catalyst) leads to very substantial *increases* in the amount of chemisorbed oxygen, thus leading to unambiguous and quantitative conclusions.

An alternative approach would have been to use potentiostatic (constant V_{WR} and $e\Phi$) rather than galvanostatic (constant I) operation during the experiments. This could lead, in principle, to establishing direct quantitative correlations between adsorption–desorption constants and $e\Phi$. However, such a potentiostatic operation leads to very significant variations in I during the experiments as V_{WR}° varies by almost 1 V upon switching from O_2 to He and then to C_2H_4. Such current variations can complicate data interpretation and thus the galvanostatic mode of operation was chosen.

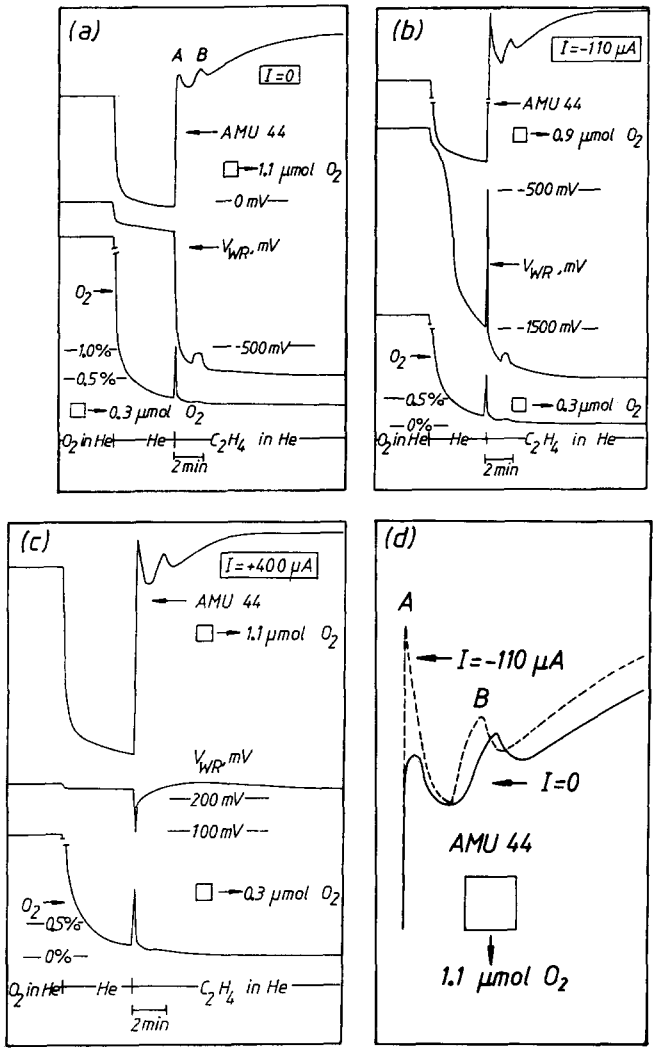

FIG. 4. Typical response of catalyst potential, effluent oxygen partial pressure, and AMU 44 signal (CO_2^+ and $C_2H_4O^+$) during isothermal titration of oxygen preadsorbed on a Ag catalyst film with C_2H_4. T = 435°C. (a) I = 0, (b) I = −110 μA, (c) I = 400 μA, (d) comparison of AMU 44 peaks for I = 0 and I = −110 μA.

RESULTS

General features. Figure 4a shows the results of a typical experiment of surface titration of oxygen by C_2H_4 for I = 0. The Ag catalyst is initially exposed to P_{O_2} = 21 kPa for a period t_{O_2} = 15 min. Then the reactor is purged with ultrapure He for a period t_{He} = 180 s. Subsequently the reactor is purged with C_2H_4 while monitoring V_{WR}, AMU 16 for O_2 and AMU 44 for C_2H_4O and CO_2. It should be noted that in Fig. 4, as well as in Fig. 5, the unavoidable high vacuum system background at AMU 44 has not been subtracted from the signal. This background noise was suppressed during t_{He}. The exit oxygen concentration was also monitored using the electrochemical oxygen analyzer.

A first interesting feature is the appearance of a sharp O_2 peak immediately after C_2H_4 introduction. This peak corresponds

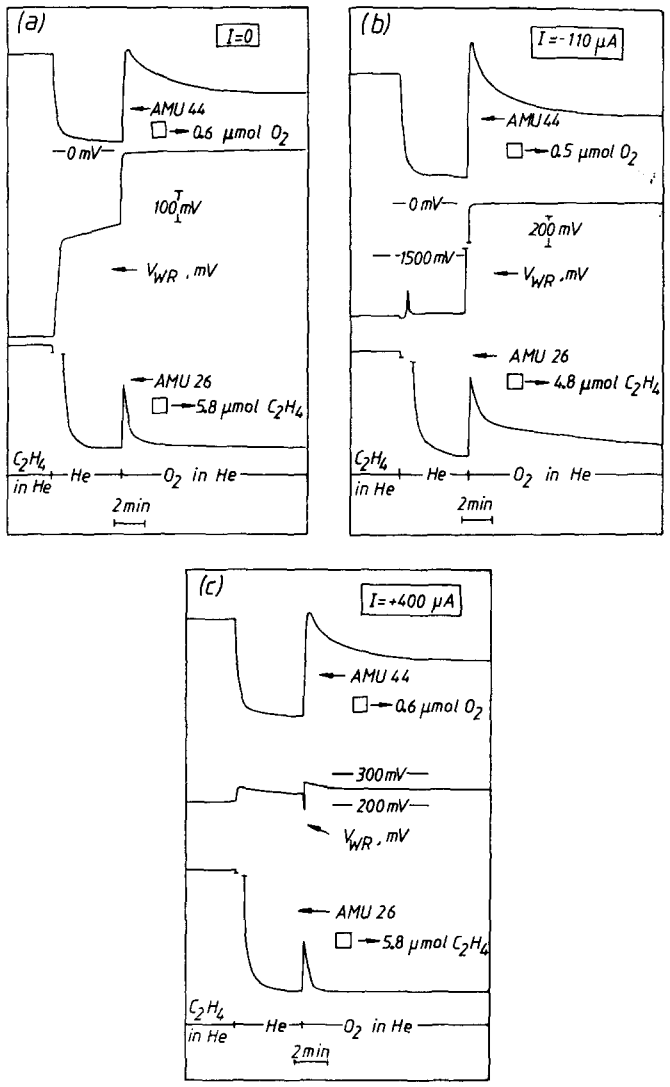

FIG. 5. Typical response of catalyst potential, AMU 44 signal (CO_2^+ and $C_2H_4O^+$) and AMU 26 signal ($C_2H_2^+$) during isothermal titration of ethylene preadsorbed on a Ag catalyst film with O_2. T = 435°C. (a) I = 0, (b) I = −110 μA, (c) I = 400 μA.

to oxygen displaced by C_2H_4 on the Ag surface and shows that oxygen and C_2H_4 adsorb, at least to some extent, competitively on the surface.

A second important feature is the appearance of two temporally distinct product peaks at AMU 44. The first peak, labeled A, appears 6 s after the oxygen displacement peak, while the second peak, labeled B, appears typically 90 s after peak A.

For I = 0 (Fig. 4a) and I = −110 μA (Fig. 4b) the appearance of peak B is always accompanied by a trapezoidal peak in V_{WR} toward more positive potentials. Such a peak in V_{WR} does not appear for I = 400 μA (Fig. 4c). The height of this trapezoidal V_{WR} peak, which for I = 0 appears for V_{WR}° values between −550 and −580 mV, increases substantially with increasing oxygen exposure time t_{O_2}. Thus the peak height increases

from 25 to 75 mV as t_{O_2} increases from 300 to 1800 s. The positive sign of this trapezoidal V_{WR} peak indicates an increase in catalyst surface work function. This together with the *simultaneously* appearing second product peak shows that the peak is due to subsurface oxygen (*19–23*, *37*) which is forced to emerge on the surface and react with C_2H_4 when chemisorbed atomic oxygen is depleted from the surface. Campbell and Paffett (*23*) have shown already that subsurface oxygen can indeed be removed from Ag by using CO to produce CO_2 at temperatures of 200 to 360°C. It can therefore be safely concluded that peak A is due to the reaction of ethylene with the β-state of chemisorbed oxygen, i.e., atomic oxygen, observed in TPD spectra (*22*), while peak B corresponds to the γ-state of oxygen, i.e., subsurface oxygen (*22*).

As shown in Fig. 4b, the overall behavior is qualitatively similar for $I = -110$ μA, except for the appearance of a very narrow V_{WR} peak. The first product peak A is, however, now significantly *larger* than that for $I = 0$ (Fig. 4d). This shows conclusively that the amount of reactive chemisorbed atomic oxygen N_O is significantly *higher* for $I = -110$ μA, i.e., for $\Delta e\Phi < 0$, than for $I = 0$. This is exactly what one expects for an electron acceptor adsorbate, such as atomic oxygen, upon decreasing substrate work function, i.e., a strengthening in the chemisorptive bond and a concomitant increase in adsorbate coverage.

Both peak A and peak B are also present for $I = 400$ μA, i.e., $\Delta e\Phi > 0$, as shown in Fig. 4c. Data interpretation is now less straightforward, since oxygen is in this case continuously supplied to the catalyst as O^{2-}. We thus do not attempt to draw any quantitative conclusions and limit the comparisons between cases a and b. It is, however, interesting to note the insensitivity of V_{WR} (and $e\Phi$) to changes in gaseous composition (Fig. 4c). This seems to indicate that oxygen is now only weakly adsorbed on the surface, as one would expect for an electron acceptor adsorbate on a high work function substrate. Consequently it appears that a significant part of the A and B peaks is due to electrochemically supplied oxygen.

Figure 5 shows typical results of surface titration of ethylene by oxygen for $I = 0$, -110, and 400 μA, respectively. In all cases there is an AMU 26 peak, corresponding to C_2H_4 displaced by oxygen upon oxygen chemisorption and *one* product peak at AMU 44 which appears some 20 s after the C_2H_4 displacement peak.

The catalyst potential behavior depends strongly on the applied current. Thus for $I = 0$ (Fig. 5a) the catalyst potential in the presence of $P_{C_2H_4} = 11$ kPa is $V^{\circ}_{WR} = -700$ mV. Upon purging with He, V°_{WR} increases, first abruptly then gradually, to -250 mV. It then reaches zero rapidly upon exposure to O_2. When $I = -110$ μA (Fig. 5b) the catalyst potential $V_{WR}(-1880$ mV for $P_{C_2H_4} = 11$ kPa) is affected very little by purging with He and quickly reaches -60 mV in presence of O_2. When $I = 400$ μA the catalyst potential is practically unaffected during the titration (Fig. 5c).

Effect of polarizing current on oxygen adsorption. Figure 6 shows the effect of oxygen exposure time t_{O_2} on the amount N_O of chemisorbed reactive atomic oxygen leading to the first product peak A. Thus the figure shows essentially the kinetics of oxygen adsorption leading to atomic oxygen, i.e.,

$$O_2(g) \rightarrow 2O(a). \qquad (9)$$

This would have been exactly the case if the results had been extrapolated to $t_{He} = 0$. Only a relatively minor distortion would have been caused in this way and we have chosen to present the raw data, i.e., N_O for a fixed small value of t_{He}, rather than the extrapolated values for $t_{He} = 0$, i.e., $N_{O,max}$.

As shown in Fig. 6, a negative current, i.e., O^{2-} *removal from* the catalyst, causes a *sixfold increase* in the amount of chemisorbed reactive oxygen for $t_{O_2} = 5$ min and a *threefold* increase for $t_{O_2} = 20$ min. These results show conclusively that the chemisorptive properties of the Ag catalyst sur-

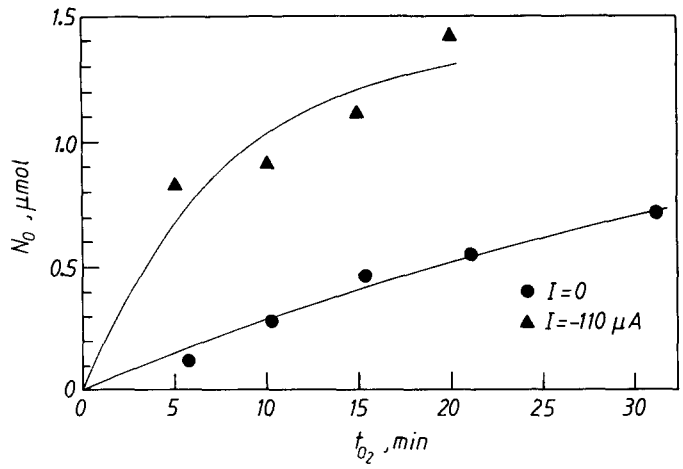

FIG. 6. Effect of applied current on the kinetics of oxygen adsorption on Ag. The figure shows the effect of the time t_{O_2} of catalyst exposure to O_2 on the amount of adsorbed reactive oxygen leading to the first product peak. T = 435°C; t_{He} = 4.5 min.

face change significantly during O^{2-} pumping and, in fact, that lowering the catalyst work function $e\Phi$ causes at least a sixfold increase in the rate of oxygen adsorption, and thus in the sticking coefficient of oxygen, and a near threefold increase in the reactive oxygen uptake of the catalyst.

It is worth noting that the above differences become even more pronounced if one attempts to take into account that atomic oxygen is being continuously removed from the catalyst at a rate of 3.4×10^{-7} g-atom O per 10 min for $I = -110$ μA.

The difference ΔV_{WR} in catalyst potential or equivalently in work function ($\Delta e\Phi = e\Delta V_{WR}$) between $I = 0$ and $I = -110$ μA varies during each titration experiment due to the galvanostatic operation. Upon comparing Figs. 4a and 4b one observes that $\Delta e\Phi$ varies typically between -0.1 eV (upon exposure to O_2) and -1.0 eV (upon titration with C_2H_4).

One can apply the standard definition of the enhancement factor Λ, i.e., Eq. (4), to the case of oxygen adsorption, i.e., reaction (9),

$$\Lambda_{ad} = \Delta r_{ad}/(I/2F), \qquad (10)$$

where Δr_{ad} is the observed increase in the rate of oxygen adsorption. The latter can be obtained from the slopes of Fig. 6. The Λ values thus computed are of the order $\Lambda_{ad} \approx -8$. Both the sign and the magnitude of Λ clearly show that the observed behavior is non-Faradaic, i.e., cannot be attributed to coverage effects.

Figure 7 shows the effect of t_{O_2} on the amount $N_{O,sub}$ of subsurface oxygen leading to the second product peak B. There is only a very small decrease in $N_{O,sub}$ for $I = -110$ μA vs $I = 0$ and this small difference can be accounted for, almost quantitatively, by the rate $I/2F$ of O^{2-} removal from the catalyst for $I = -110$ μA (Fig. 7). As shown in Fig. 8, $N_{O,sub}$ varies linearly $t_{O_2}^{1/2}$. A similar observation has been reported by Haul and Neubauer (*29*). This also provides strong evidence that peak B is indeed due to subsurface oxygen and that the rate of subsurface oxygen formation is limited by the diffusion of atomic oxygen in the Ag lattice, as further analyzed under Discussion.

Effect of polarizing current on oxygen desorption. Figure 9 shows the effect of oxygen desorption time t_{He} on the amount of chemisorbed reactive oxygen N_O leading to the first product peak A. Thus Fig. 9 essentially depicts the kinetics of the atomic oxy-

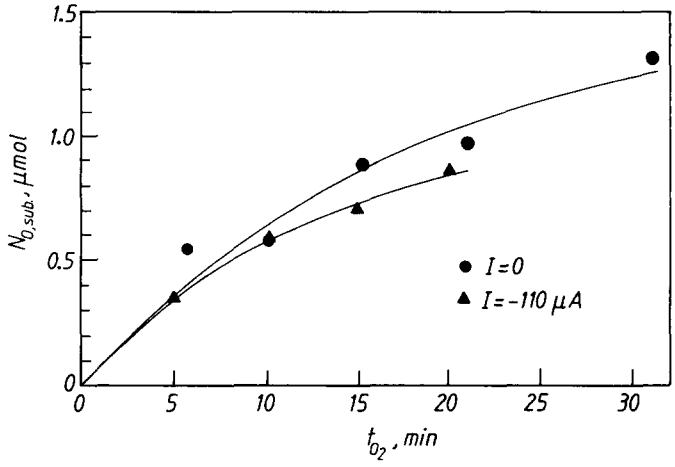

FIG. 7. Effect of applied current on the kinetics of oxygen adsorption on Ag. The figure shows the effect of the time t_{O_2} of catalyst exposure to O_2 on the amount of adsorbed reactive oxygen leading to the second product peak (subsurface oxygen); T = 435°C; t_{He} = 4.5 min.

gen desorption reaction:

$$2\ O(a) \rightarrow O_2(g). \qquad (11)$$

As shown in the figure, the desorption data can be adequately described by a pseudo-first-order rate expression, in agreement with previous studies on similar Ag films (*49*, *50*), although a second-order desorption rate expression, which is suggested by many TPD results (*19*, *22*), could also provide a

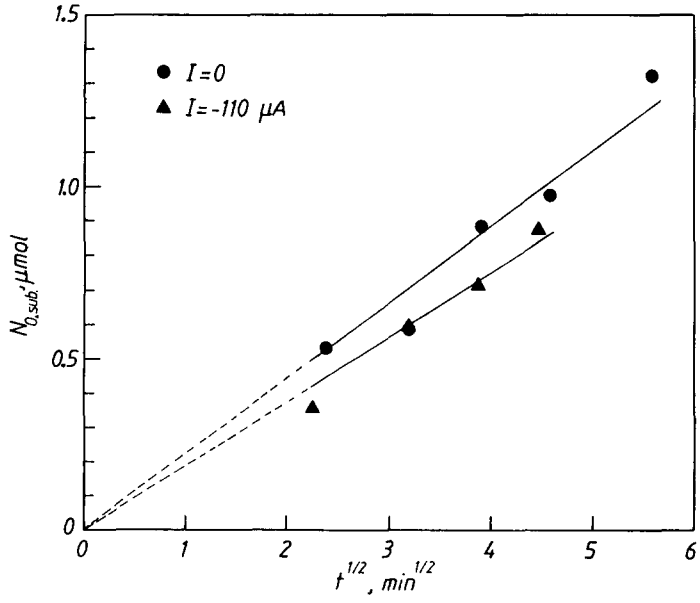

FIG. 8. Dependence of the amount of subsurface oxygen leading to second product peak on $t_{O_2}^{1/2}$. T = 435°C, t_{He} = 4.5 min.

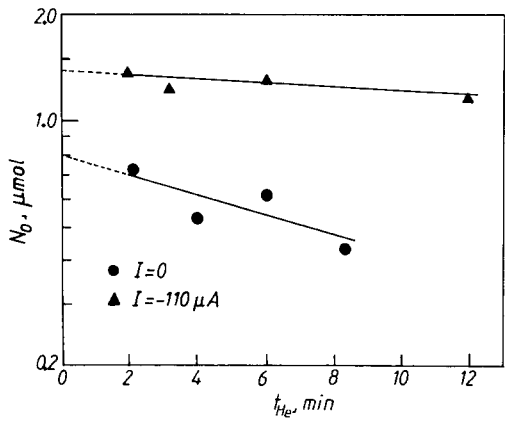

FIG. 9. Effect of applied current on the kinetics of oxygen desorption from Ag. The figure shows the effect of the time of catalyst exposure to ultrapure He on the amount of adsorbed reactive oxygen leading to the first product peak T = 435°C; t_{O_2} = 15 min.

reasonable fit. Using the $N_{O,max}$ value for $I = 0$ and assuming a 1:2 atomic O to Ag adsorption stoichiometry (*19*), one computes $A = 0.13$ m^2 for the surface area of the Ag film.

The main observation is that decreasing catalyst work function $e\Phi$ ($I = -110$ μA) causes a significant, i.e., twofold, increase in the maximum reactive oxygen uptake $N_{O,max}$ and a fivefold decrease in the first-order desorption rate constant k_d. Thus for $I = 0$, $N_{O,max} = 1.6 \times 10^{-6}$ g-atom O, $k_d = 1.1 \times 10^{-3}$ s^{-1}, while for $I = -110$ μA, $N_{O,max} = 2.9 \times 10^{-6}$ g-atom O, $k_d = 0.22 \times 10^{-3}$ s^{-1}. Both the increase in $N_{O,max}$ and the decrease in k_d indicate a significant strengthening of the silver–atomic oxygen chemisorptive bond.

Applying again the standard definition of Λ to the oxygen desorption reaction (11), i.e.,

$$\Lambda_d = \Delta r_d/(I/2F), \qquad (12)$$

where Δr_d is the observed increase (<0) in the rate of oxygen desorption upon current imposition, one can use Fig. 7 to compute Λ_d values of the order of 9.

Similar to the case of oxygen adsorption kinetics, the polarizing current was found to have a negligible effect on $N_{O,sub}$ for fixed t_{He}. Interestingly, $N_{O,sub}$ was found to increase slowly with increasing t_{He} (*48*). This is due to the finite level of oxygen impurity in the cell reactor during He purging, which is of the order of 10 ppm as computed from the open-circuit cell potential V°_{WR} via the Nernst equation,

$$V^{\circ}_{WR} = (RT/4F)\ln(P_{O_2}/0.21), \qquad (13)$$

where P_{O_2} is the oxygen impurity partial pressure and 0.21 is the oxygen partial pressure on the air reference side of the solid electrolyte cell. Equation (13) is valid to the extent that no catalytic reaction is taking place on the catalyst (*2*, *49*, *50*), which is certainly the case during He purging. Therefore subsurface oxygen could only be removed by catalyst exposure to C_2H_4 to form peak B.

Adsorption and desorption of ethylene. Polarizing current was found to have only a very small effect on the kinetics of ethylene adsorption and desorption (*48*). Both $I > 0$ and $I < 0$ appear to cause a small (<30%) enhancement in the adsorption kinetics (*48*) but the effect is almost negligible in comparison with the case of oxygen (Figs. 6 and 9).

DISCUSSION

The present work shows conclusively that the chemisorptive properties of Ag are significantly and reversibly affected upon polarizing the Ag–solid electrolyte interface. The main result is that decreasing the catalyst $e\Phi$ by a few hundred millivolts ($I = -110$ μA) causes

1. A more than sixfold increase in the sticking coefficient or rate of atomic oxygen adsorption (Fig. 6).
2. A more than fivefold decrease in the rate of atomic oxygen desorption (Fig. 9).
3. A twofold increase in the equilibrium atomic oxygen catalyst uptake (Fig. 9).

An additional result is that the amount of subsurface oxygen varies linearly with the square root of the time of catalyst exposure to O_2, $t_{O_2}^{1/2}$ (Fig. 8), as already reported by

Haul and co-workers (*29*), and that this amount is not affected significantly by the changing catalyst work function.

The above observations strongly corroborate the validity of the proposed interpretation of the NEMCA effect (*1–17*) by establishing that decreasing catalyst work function, via polarization of the metal–solid electrolyte interface, strengthens significantly the chemisorptive bond of atomic oxygen on Ag. These observations are also in good qualitative agreement with the literature, with respect to both the main types of oxygen present on and below Ag surfaces at elevated temperatures and the effect of electropositive promoters, causing a decrease in catalyst work function on the binding state of atomic oxygen on supported Ag catalysts (*35*), as discussed below.

Previous studies of the adsorption of oxygen on Ag (*19–40*) and in particular the use of TPD (*19*, *22*, *29*), isotope exchange (*19*, *22*), and XPS (*22*, *23*, *31*, *32*) have clearly established the existence of three main types of oxygen, namely molecular, atomic, and subsurface oxygen.

Molecular oxygen, usually described as α-state oxygen in TPD spectra (*22*), has been shown by Lambert and co-workers to be a spectator species, not directly involved in ethylene epoxidation. This is also supported by a recent *in situ* SERS study (*46*). The amount of molecular oxygen increases with increasing subsurface oxygen (*19*) and with increased dosing of alkali promoters (*33*). Its desorption temperature has been a matter of debate but is certainly lower than 210°C (*19*). Its low desorption temperature and low reactivity with C_2H_4 explain why no product peak corresponding to molecular oxygen was observed in the present study.

Atomic oxygen, i.e., β-state oxygen in TPD spectra (*22*), is currently believed to be responsible for both the epoxidation and the complete oxidation of C_2H_4 (*19*, *34*). Its TPD peak is usually centered near 350°C (*19*) and it rapidly exchanges with subsurface oxygen (*19*). It is clearly the type of oxygen giving rise to the first product peak A in the present experiments (Fig. 4).

It has been shown both by Dean and Bowker (*35*) and by Kitson and Lambert (*33*) that alkali promoters, causing a work function decrease $\Delta e\Phi$ up to -2 eV, also result in a significant strengthening in the bonding of atomic oxygen (*33*, *35*). Dean and Bowker (*35*) have found a 300-fold increase in the sticking coefficient, which is typically 10^{-5}–10^{-3}, and a 20–70K increase in the peak desorption temperature. These observations are in good qualitative agreement with the present work and are to be expected for an electron-acceptor adsorbate, such as atomic oxygen, when the substrate work function decreases (*2*). It is worth noting that the addition of Cl, which increases $e\Phi$, has been shown not only to block atomic oxygen sites (*19–21*) but also to weaken the atomic oxygen–Ag bond (*32*, *36*).

Subsurface oxygen, i.e., γ-state oxygen in TPD spectra (*22*), has been shown to affect significantly the chemisorptive properties of Ag surfaces (*19*). Its presence is a necessary condition for obtaining high selectivity during ethylene epoxidation. It gives a broad TPD peak centered near 600°C (*22*), rapidly exchanges with atomic oxygen, and can be cleaned off by reaction with CO (*23*) or with C_2H_4 as shown in this work. The observation that the changing work function $e\Phi$ has practically no effect on the amount of subsurface oxygen (Figs. 7 and 8) is quite reasonable. Figure 8 strongly suggests that, as previously proposed (*29*), the rate of subsurface oxygen formation is controlled by bulk diffusion of oxygen originating from the gas phase while electrochemical formation of subsurface oxygen, which is limited to $I/2F$, is negligible under the conditions of the present experiments (Fig. 7). Thus no equilibrium or even steady state is attained for subsurface oxygen during these experiments and $N_{O,sub}$ is determined by the gaseous oxygen pressure during t_{O_2} and by the bulk diffusivity of oxygen in Ag. The latter should clearly be unaffected by changing the catalyst potential and work function.

It is interesting to note that material scientists have studied for years the dissolution of oxygen in solid Ag utilizing Y_2O_3-stabilized-ZrO_2 galvanic cells (*45*). Thus both the solubility and the diffusivity of oxygen in Ag have been measured as a function of temperature between 750 and 950°C (*45*). It is not clear if the "dissolved" oxygen of material scientists (*45*) is the same oxygen species as the subsurface oxygen of surface scientists (*19*). In any case it is very likely that slow variations in the amount of subsurface or dissolved oxygen during catalyst operation cause the well-known "sluggish" transient response of the rates of ethylene epoxidation and oxidation to CO_2 upon imposition of step changes in gaseous composition and also affect, to some extent, the observed kinetics of oxygen adsorption and desorption on Ag (*26*, *27*, *49*, *50*).

The observation that changing catalyst work function has only a small effect on the adsorption and desorption of ethylene seems to imply that the chemisorptive bond of ethylene is weak and not very polar, as in addition to the donation of electrons from filled π bonding orbitals to the metal there is a finite backdonation to unoccupied π^* levels. The fact that the bond is not very polar is also shown by the relatively small (< -0.35 eV) change in the work function of Ag caused by ethylene adsorption (*41*).

Little is known about the exact nature and coverage of the spillover oxide species supplied to and removed from the catalyst surface upon electrochemical supply and removal of O^{2-} to and from the catalyst, respectively. Arakawa *et al.* (*51*, *52*) have used *in situ* XPS to investigate Ag electrodes subject to electrochemical O^{2-} pumping through a stabilized ZrO_2 disc and showed the appearance of an O 1*s* signal corresponding to ionically bonded oxygen during O^{2-} pumping. It is very likely that this signal corresponds to the spillover oxygen species causing NEMCA (*2*). A detailed *in situ* spectroscopic investigation of catalyst surfaces subject to NEMCA conditions could further elucidate this point.

SUMMARY

The chemisorptive properties of Ag for atomic oxygen can be markedly affected via NEMCA. Decreasing catalyst work function causes a sixfold increase in the rate of atomic oxygen adsorption, a fivefold decrease in its rate of desorption, and a twofold increase in its equilibrium coverage. The effect is qualitatively similar to that of alkali promoters and underlines the fact that solid electrolytes can be used as active catalyst supports to influence the chemisorptive and catalytic properties of metals in a pronounced, reversible, and, to some extent, predictable manner. Current work is focusing on the systematic study of the effect of NEMCA on the selectivity of ethylene epoxidation.

APPENDIX: WORK FUNCTION, FERMI LEVEL, AND NEMCA

The purpose of this Appendix is to analyze whether NEMCA can be discussed in terms of changes in catalyst Fermi level E_F, as suggested by one of our reviewers, instead of changes in the catalyst surface work function $e\Phi$ (Φ is the extraction potential (*2*)), as done in this and previous NEMCA studies (*1–17*).

The central finding of these studies (*1–17*) is that over wide ranges of average catalyst surface work function $e\Phi$ (typically 0.3–1.0 eV), catalytic rates r depend exponentially on $e\Phi$ and catalytic activation energies E vary linearly with $e\Phi$,

$$\ln(r/r_o) = \alpha e(\Phi - \Phi^*)/k_bT \qquad \text{(A1)}$$

$$E = E^o + \alpha_H(\Phi - \Phi^*), \qquad \text{(A2)}$$

where α, Φ^*, E^o, and α_H are reaction- and catalyst-specific constants. Equation (A1) has been found to be satisfied in over 20 catalytic reactions (*1–17*). The activation energy dependence on $e\Phi$ has been studied so far for only 6 of these reactions (*1*, *2*) but in all cases excellent agreement with (A2) has been observed.

Equations (A1) and (A2) have been extracted using NEMCA by interfacing a po-

rous metal catalyst film with a solid electrolyte (YSZ, an O^{2-} conductor or β''-Al_2O_3, a Na^+ conductor) and by using a potentiostat to vary the ohmic-drop-free potential V_{WR} of the catalyst (W, for "working" electrode) with respect to a reference (R) electrode. It has been shown both theoretically (*2*, *5*, *6*) and experimentally by means of a Kelvin probe (*1*, *10*, *11*) that

$$e\Delta V_{WR} = \Delta e\Phi, \qquad \text{(A3)}$$

where $e\Phi$ is the (average) work function of the gas-exposed (i.e., catalytically active) catalyst film surface. The derivation of Eq. (A3) has been presented in detail elsewhere (*2*, *5*). There are two points deserving some emphasis here. First, for the gas-exposed (i.e., catalytically active) catalyst surface the average outer (or Volta) potential Ψ is zero, i.e., the catalytically active surface carries no net charge under NEMCA conditions. Due to simple electrostatic considerations (*2*, *5*), all the extra charge on the catalyst film must remain localized at the metal–solid electrolyte interface. This is the key step in deriving theoretically the experimentally extracted (*1*, *10*, *11*) Eq. (A3). Second, physically, the change in work function $\Delta e\Phi$ upon changing the ohmic-drop-free catalyst potential by ΔV_{WR} is due to the spillover of ions from (or to) the solid electrolyte to (or from) the catalyst surface. These spillover ions (together with their compensating charge in the metal, thus forming spillover dipoles) spread onto the catalyst surface changing its work function by $\Delta e\Phi = e\Delta V_{WR}$ and its chemisorptive and catalytic properties according to Eqs. (A1) and (A2).

Although Eqs. (A1) and (A2) have been extracted using NEMCA, i.e., by utilizing the ability of solid electrolytes to act as convenient and reversible promoter ion donors, there is no reason to expect that the validity of Eqs. (A1) and (A2) is limited to metal films interfaced with solid electrolytes. For example, the work of Surnev (*53*) has shown that the sticking coefficient of oxygen on alkali-doped Ge increases exponentially with the alkali-induced work function change regardless of alkali type. Thus the results of Surnev (*53*) obtained without using any solid electrolyte, conform to Eq. (A1). Comparative NEMCA studies of C_2H_4 oxidation on Pt using different types of solid electrolytes and promoting ions have also shown very good agreement with Eq. (A1), although the α coefficients were found to differ by up to a factor of two from one type of promoting ion to another (*2*, *5*, *10*). We also provide a second example showing the broader range of validity of Eqs. (A1) and (A2): The average initial dipole moment of Na introduced on polycrystalline Pt catalyst films under NEMCA conditions (*10*, *11*) was found to be 2.15×10^{-29} C·m or 6.5 D, i.e., almost identical to the value measured for Na on a clean Pt(111) surface (*54*, *55*), where Na had been introduced from the gas phase via a standard metal dispenser source. Thus the origin of Na plays no role on its final state on the Pt surface and, therefore, on the catalytic changes it induces. Consequently, since Eq. (A1) was obeyed for C_2H_4 oxidation on Pt upon using β''-Al_2O_3 as the Na source (*2*, *10*), it follows that Eq. (A1) would also be obeyed if a metal dispenser source had been used to supply Na on a Pt catalyst sample *not interfaced* with a solid electrolyte, as in the work of Surnev (*53*). The solid electrolyte provides the additional convenience of controlled, reversible, and in some cases unique (e.g., oxygen spillover species in the YSZ case) introduction of measurable (via Faraday's law (*2*, *10*, *11*)) amounts of dopant on catalyst surfaces.

It therefore appears that Eqs. (A1) and (A2) are not limited to the case where the metal catalyst is interfaced with a solid electrolyte (NEMCA conditions), but may describe, at least for several classes of catalytic systems, the effect of promoters on catalytic activity in terms of the promoter-induced work function change.

One can then analyze the extent to which it is possible to use changes in catalyst Fermi level E_F, instead of changes in catalyst surface work function $e\Phi$, to describe the in-

duced changes in catalytic rate [Eq. (A1)] and activation energy [Eq. (A2)].

The Fermi level of a metal is identical with the electrochemical potential of electrons $\overline{\mu}$ in the metal (*56*), i.e.,

$$E_F = \overline{\mu}. \tag{A4}$$

The latter is linearly related to the work function $e\Phi$ via (*55–61*)

$$-\overline{\mu} = e\Phi + e\Psi. \tag{A5}$$

The work function is the work required to bring an electron from the Fermi level of the metal to a point outside the metal surface, where the image forces are negligible, typically 10^{-4} to 10^{-5} cm outside the metal surface (*55, 57*). The Volta (or outer) potential Ψ at this point is defined so that $e\Psi$ is the energy required to bring the electron from that point to an "infinite" distance from the metal surface at its ground state (*57, 60–62*). It is worth emphasizing that $\overline{\mu}$ is a spatially uniform property in the metal sample but $e\Phi$ and Ψ (which are both accessible to experimental measurement) are *not,* in general, spatially uniform over the metal sample surface. Different crystallographic planes are well known to have different $e\Phi$ and $e\Psi$ values and thus nontrivial variations in $e\Phi$ and $e\Psi$ are to be expected on the surface of polycrystalline samples (*55, 57–59*). It is, however, important to note that the sum of $e\Phi$ and $e\Psi$ is, in view of Eq. (A5), spatially uniform. As shown in detail elsewhere Eq. (A1) and (A2) apply to the, appropriately defined, average catalyst surface $e\Phi$ and $e\Psi$ (*2*).

For the gas-exposed (i.e., catalytically active) surface of metal films interfaced with solid electrolytes, $\Psi = 0$; thus Eq. (A5) reduces to $-\overline{\mu} = e\Phi$. Consequently for metal films interfaced with solid electrolytes and subject to NEMCA conditions one can rewrite Eqs. (A1) and (A2) in the form

$$\ln(r/r_o) = -\alpha(\overline{\mu} - \overline{\mu}^*)/k_bT \tag{A6}$$

$$E = E^o - \alpha_H(\overline{\mu} - \overline{\mu}^*). \tag{A7}$$

Equations (A6) and (A7) are equivalent to Eqs. (A1) and (A2) provided $\Psi = 0$, a condition which is certainly met for the gas-exposed surfaces of catalyst films interfaced with solid electrolytes as in NEMCA experiments.

However, contrary to Eqs. (A1) and (A2), Eqs. (A6) and (A7) are not valid for the more general case of an arbitrary metal catalyst sample. To illustrate this we provide two examples.

First consider an unsupported and initially uncharged metal (e.g., Pt) catalyst sphere of radius R. As shown by Eq. (A5) there are, conceptually and experimentally, two different ways to change the electrochemical potential $\overline{\mu}$ of electrons in the sphere by, say, 1 eV. One involves changing $e\Phi$, e.g., decreasing $e\Phi$ by 1 eV, via dipole formation on its surface (e.g., by adsorbing Na at a coverage of the order of $\theta_{Na} \sim 0.05$ to 0.1 (*10, 11, 55*)). The other involves changing $e\Psi$ by 1 eV, i.e., by introducing on the sphere a net charge q so that the outer potential Ψ changes by $\Delta\Psi = -1$ V. In this case it follows from elementary electrostatics that the surface charge coverage θ_c defined from

$$\theta_c = \frac{(q/e)}{N_s \cdot 4\pi R^2}, \tag{A8}$$

where N_s is the surface concentration of metal atoms ($\sim 10^{19}$ atoms/m^2) and $e = 1.6 \times 10^{-19}$ C, will equal

$$\theta_c = \frac{\varepsilon_o \Delta\Psi}{eN_sR}, \tag{A9}$$

where $\varepsilon_o = 8.85 \times 10^{-12}$ C^2/J/m. Thus for a sphere of radius 1 mm or 1 μm, the surface coverage θ_c equals 5.5×10^{-9} or 5.5×10^{-6}, respectively.

It is therefore obvious that in the former case ($\overline{\mu}$ change due to Na adsorption $\theta_{Na} \sim$ 0.05 to 0.1) the catalytic properties of the sphere will change significantly, in accordance with Eqs. (A1) and (A2) as in NEMCA studies (*1–17*), while in the latter case ($\overline{\mu}$ change due to charging) nothing will happen to the catalytic properties of the sphere, since θ_c is practically zero.

As a second example consider that in the experimental setup used in this and in previous NEMCA studies the solid electrolyte is replaced, conceptually, by vacuum or by a perfect insulator and that a potentiostat is used to charge the catalyst film by 1 V. In this case there will be no spillover species and $\overline{\mu}$ will change by 1 eV, but since $e\Psi$, and not $e\Phi$, will change by 1 eV, there will be no effect on catalytic rate. Stated differently, simple charging of a metal sample does not induce NEMCA. Charge effects can, of course, become important when the field strength on the catalyst surface is of the order of 10^{10} V/m (*63*). Such field strengths are also well known to change $e\Phi$ (*55*).

In summary, replacement of Eqs. (A1) and (A2) by Eqs. (A6) and (A7) is, in general, not valid. It is the work function change and not the Fermi level change which can be related to changes in catalytic activity.

We make a final note on Eqs. (A1) and (A2). It has been argued that they support the importance of "long-range" electronic effects in promotion and catalysis (*1*, *18*). The extent to which this may be valid has been discussed elsewhere (*2*). It is, however, worth pointing out that equations which are formally very similar to Eqs. (A1) and (A2) (with $e\Phi$ replaced by the metal potential V, e.g., the Butler–Volmer Equation (*2*, *62*)) have been well known for many years to describe the dependence of *electrocatalytic* rates and activation energies on V, without taking this to necessarily imply that only long-range electronic effects are important in electrocatalysis. It is very likely that Eqs. (A1) and (A2) simply underline that nearly every bond broken or formed in the rate-limiting step of a catalytic reaction has a certain ionic character.

ACKNOWLEDGMENTS

Financial support from the EEC Non-Nuclear Energy programme is gratefully acknowledged. One of the authors (C.G.V.) thanks the Alexander von Humboldt Foundation of Germany for a fellowship.

REFERENCES

1. Vayenas, C. G., Bebelis, S., and Ladas, S., *Nature (London)* **343**(6259), 625 (1990).
2. Vayenas, C. G., Bebelis, S., Yentekakis, I. V., and Lintz, H.-G., *Catal. Today* **11**(3), 303 (1992).
3. Yentekakis, I. V., and Vayenas, C. G., *J. Catal.* **111,** 170 (1988).
4. Vayenas, C. G., Bebelis, S., and Neophytides, S., *J. Phys. Chem.* **92,** 5083 (1988).
5. Bebelis, S., and Vayenas, C. G., *J. Catal.* **118,** 125 (1989).
6. Neophytides, S., and Vayenas, C. G., *J. Catal.* **118,** 147 (1989).
7. Vayenas, C. G., Bebelis, S., Neophytides, S., and Yentekakis, I. V., *Appl. Phys. A* **49,** 95 (1989).
8. Vayenas, C. G., Bebelis, S., Yentekakis, I. V., Tsiakaras, P., and Karasali, H., *Platinum Met. Rev.* **34**(3), 122 (1990).
9. Vayenas, C. G., and Neophytides, S., *J. Catal.* **127,** 645 (1991).
10. Vayenas, C. G., Bebelis, S., and Despotopoulou, M., *J. Catal.* **128,** 415 (1991).
11. Ladas, S., Bebelis, S., and Vayenas, C. G., *Surf. Sci.* **251/252,** 1062 (1991).
12. Lintz, H-G., and Vayenas, C. G., *Angew. Chem.* **101,** 725 (1989); *Angew. Chem. Int. Ed. Engl.* **28,** 708 (1989).
13. Vayenas, C. G., Bebelis, S., and Neophytides, S., *in* "Studies in Surface Science and Catalysis" (G. Centi and P. Trifiro, Eds.), Vol. 55, pp. 643–652. Elsevier, Amsterdam, 1990.
14. Vayenas, C. G., Bebelis, S., Yentekakis, I. V., Tsiakaras, P., Karasali, H., and Karavasilis, Ch., *ISSI Lett.* **2,** 5 (1991).
15. Vayenas, C. G., Bebelis, S., and Kyriazis, C., *Chemtech* **21,** 500 (1991).
16. Bebelis, S., Karavasilis, Ch., Karasali, H., Tsiakaras, P., Yentekakis, I. V., and Vayenas, C. G., *in* "Proceedings, 2nd International Symposium on Solid Oxide Fuel Cells, Athens, Greece, 1990," pp. 353–360. EEC, Luxembourg, 1991.
17. Vayenas, C. G., Bebelis, S., Yentekakis, I. V., Tsiakaras, P., Karasali, H., and Karavasilis, Ch., *in* "Proceedings, 3rd International Symposium on Systems with Fast Ionic Transport, Holzhau, Germany, 1991," *Mater. Sci. Forum* **76,** 141 (1991); Tsiakaras, P., and Vayenas, C. G., *Mater. Sci. Forum* **76,** 179 (1991); Karasali, H., and Vayenas, C. G., *Mater. Sci. Forum* **76,** 171 (1991); Karavasilis, Ch., Bebelis, S., and Vayenas, C. G. *Mater. Sci. Forum* **76,** 175 (1991); Bebelis, S., and Vayenas, C. G., *Mater. Sci. Forum* **76,** 221 (1991).
18. Pritchard, J., *Nature (London)* **343**(6259), 592 (1990).
19. Van Santen, R. A., and Kuipers, H. P. C. E., *Adv. Catal.* **35,** 265 (1987).
20. Sachtler, W. M. H., Backx, C., and Van Santen, R. A., *Catal. Rev. Sci. Eng.* **23,** 127 (1981).
21. Verykios, X. E., Stein, F. P., and Coughlin, R. W., *Catal. Rev. Sci. Eng.* **22,** 197 (1980).
22. Grant, R. B., and Lambert, R. M. *Surf. Sci.* **146,** 256 (1984).

23. Campbell, C. T., and Paffett, M. T., *Surf. Sci.* **143,** 517 (1984).
24. Prince, K. C., Paolucci, G., and Bradshaw, A. M., *Surf. Sci.* **175,** 101 (1986).
25. Barteau, M. A., and Madix, R. J., *Chem. Phys. Lett.* **97,** 85 (1983).
26. Czanderna, A. W., *J. Phys. Chem.* **68,** 2765 (1964).
27. Anderson, K. L., Plischke, J. K., and Vannice, M. A., *J. Catal.* **128,** 148 (1991).
28. Benndorf, C., Franck, M., and Thieme, F., *Surf. Sci.* **128,** 417 (1983).
29. Haul, R., and Neubauer, G., *J. Catal.* **105,** 39 (1987).
30. Haul, R., Hoge, D., Neubauer, G., and Zeeck, U., *Surf. Sci. Lett.* **122,** L622 (1982).
31. Peuckert, M., *Surf. Sci.* **146,** 329 (1984).
32. Kitson, M., and Lambert, R. M., *Surf. Sci.* **109,** 60 (1981).
33. Kitson, M., and Lambert, R. M., *Surf. Sci.* **110,** 205 (1981).
34. Tan, S. A., Grant, R. B., and Lambert, R. M., *J. Catal.* **106,** 54 (1987).
35. Dean, M., and Bowker, M., *J. Catal.* **115,** 138 (1989).
36. Rovida, G., Pratesi, F., and Ferroni, E., *J. Catal.* **41,** 140 (1976).
37. Van den Hoek, P. J., Baerends, E. J., and Van Santen, R. A., *J. Phys. Chem.* **93,** 6469 (1989).
38. Stoukides, M., and Vayenas, C. G., *J. Catal.* **70,** 137 (1981).
39. Karavasilis, Ch., Bebelis, S., and Vayenas, C. G., in preparation.
40. Jorgensen, K. A., and Hoffmann, R., *J. Phys. Chem.* **94,** 3046 (1990).
41. Schmiedl, E., Wissmann, P., and Wittmann, E., *Surf. Sci.* **135,** 341 (1983).
42. Vayenas, C. G., Ioannides, A., and Bebelis, S., *J. Catal.* **129,** 67 (1991).
43. Robertson, N. L., and Michaels, J. N., *J. Electrochem. Soc.* **137**(1), 129 (1990).
44. Wang, D. Y., and Nowick, A. S., *J. Electrochem. Soc.* **126**(7), 1155 (1979); **126**(7), 1166 (1979); **128**(1), 55 (1981).
45. Ramanarayanan, T. A., and Rapp, R., *Metal. Trans.* **3,** 3239 (1972).
46. Boghosian, S., Bebelis, S., Vayenas, C. G., and Papatheodorou, G. N., *J. Catal.* **117,** 561 (1989).
47. Yentekakis, I. V., Neophytides, S., and Vayenas, C. G., *J. Catal.* **111,** 152 (1988).
48. Bebelis, S., Ph.D. thesis, University of Patras, 1989.
49. Stoukides, M., and Vayenas, C. G., *J. Catal.* **64,** 18 (1980).
50. Stoukides, M., and Vayenas, C. G., *J. Catal.* **82,** 45 (1983).
51. Arakawa, T., Saito, A., and Shiokawa, J., *Chem. Phys. Lett.* **94,** 250 (1983).
52. Arakawa, T., Saito, A., and Shiokawa, J., *Appl. Surf. Sci.* **16,** 365 (1983).
53. Surnev, L., *Surf. Sci.* **11,** 458 (1981).
54. Schröder, W., and Hölzl, J., *Solid State Commun.* **24,** 777 (1977).
55. Hölzl, J., and Schulte, F. K., *in* "Solid Surface Physics," pp. 1–150. Springer-Verlag, Berlin, 1979.
56. Reiss, H. J., *J. Phys. Chem.* **89,** 3783 (1985); *J. Electrochem. Soc.* **135,** 247C (1988).
57. Gundry, P. M., and Tompkins, F. C., *in* "Experimental Methods in Catalytic Research" (R. B. Anderson, Ed.), pp. 100–168. Academic Press, New York, 1968.
58. Trasatti, S., *in* "Advances in Electrochemistry and Electrochemical Engineering" (H. Gerischer and Ch. W. Tobias, Eds.), Vol. 10, pp. 215–321. Wiley, New York, 1977.
59. Ashcroft, N. W., and Mermin, N. D., *in* "Solid State Physics," pp. 354–371. Hott–Saunders Intl. Eds., Boston, 1976.
60. Lamy, C. *in* "Propriétés électriques des interfaces chargées" (D. Schuhmann, Ed.), pp. 210–241. Masson, Paris, 1978.
61. Amariglio, H., *J. Chim. Phys.* **64,** 1391 (1967).
62. Bockris, J. O'M., and Reddy, A. K. N. "Modern Electrochemistry," Vol. 2. Plenum, New York, 1970.
63. Block, J. H., Kreuzer, H. J., and Wang, L. C., *Surf. Sci.* **246,** 125 (1991).